Advanced light management techniques for two-terminal hybrid tandem solar cells

Blanker, A.J.; Berendsen, P.; Phung, N.; Vroon, Z.E.A.P.; Zeman, M.; Smets, A.H.M.

Important note
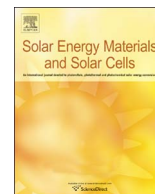To cite this publication, please use the final published version (if applicable).
Please check the document version above.

Contents lists available at ScienceDirect

Solar Energy Materials and Solar Cells

journal homepage: www.elsevier.com/locate/solmat

Advanced light management techniques for two-terminal hybrid tandem solar cells

A.J. Blanker[a,*], P. Berendsen[a], N. Phung[a], Z.E.A.P. Vroon[b], M. Zeman[a], A.H.M. Smets[a]

[a] Delft University of Technology, Mekelweg 4, Delft, Netherlands
[b] TNO/Solliance, HTC 21, Eindhoven, Netherlands

ARTICLE INFO

ABSTRACT

Multi-junction solar cells are considered for various applications, as they tackle various loss mechanisms for single junction solar cells. These losses include thermalization and non-absorption below the band gap. In this work, a tandem configuration comprising copper-indium-gallium-di-selenide (CIGS) and hydrogenated amorphous silicon (a-Si:H) absorber layers is studied. Two main challenges are addressed in this work. Firstly, the natural roughness of CIGS is unfavorable for monolithically growing a high quality a-Si:H top cell. Some sharp textures in the CIGS induce shunts in the a-Si:H top junction, limiting the electrical performance of such a configuration. To smoothen this interface, the possibility of mechanically polishing the intermediate i-ZnO layer has been explored. The second challenge that is addressed, is the significant current mismatch in these tandem architectures. To enhance absorption in the current-limiting top cell, the ZnO:Al front electrode was textured by means of wet-etching the entire tandem stack. We demonstrated that one can manipulate the morphology of the random textures by varying the growth conditions of the ZnO:Al, leading to better light management in these devices.

1. Introduction

Thin-film technologies can have certain attractive characteristics in terms of weight, shapes, and possible translucence. In search for higher voltages and efficiencies, much research has focused on multi-junction thin-film photovoltaic devices. This is not limited to the field comprising III-V semiconductors, but also thin-film technology materials have been extensively researched. Combining a-Si:H with nanocrystalline silicon – the micromorph solar cells – has widely been investigated [1], but also work on (all silicon-based) triple-junction [2] and even quadruple junction solar cells are found in literature [3,4]. Likewise, multi-junction configurations are considered in the field of organic photovoltaics [5,6]. Beyond that, merging of different photovoltaic technologies in so-called hybrid multi-junctions is also being explored. Recent development are found in combining one junction of crystalline silicon with a junction of perovskite [7] or III-V semiconductors [8]. In addition, in the field of CIGS such stacks have been proposed, including combining this junction with various dye sensitized solar cells [9–11]. In this latter field, an additional incentive is to limit the use of the relatively scarce Indium. Using multi-junction devices, thinner CIGS layer can generate higher photo-conversion efficiencies, due to both higher voltages obtained in thinner absorber layers [12,13], as well as the better spectral utilization.

In terms of contact and interconnection design, multi-junction devices can be categorized in two configurations; two-terminal and four-terminal devices. The challenge for four-terminal multi-junction devices lies in the complex electrical components required for the integration of these cells in modules and complete systems. The challenge for two-terminal devices is to accomplish a design in which top cell and bottom cell are close to current matching while preserving a high value for the fill factor (*FF*). Consequently, two-terminal configurations face the biggest challenges in the design and fabrication of the cells.

This work focuses on two-terminal double-junction devices, where all layers are monolithically integrated. In these devices, two PV cells based on semiconductor absorber layers with different energetic bandgaps are stacked, with the cell based on the widest bandgap material facing the front side at which the irradiance is incident. In such a tandem cell the photons have - on average - less excess energy relative to the bandgaps, reducing thermalization losses, and thereby resulting in a more efficient utilization of the solar spectrum.

CIGS is a direct bandgap material with a high absorption coefficient till close to its band gap around 1.2 eV. This makes CIGS a suitable semiconductor material to function as a bottom cell in these devices. The amorphous silicon solar cell technology regards a wide bandgap

---

* Corresponding author.
E-mail address: a.j.blanker@tudelft.nl (A.J. Blanker).

material (1.66 eV), is well-developed, and is processed at a temperature below 200 °C. These properties making a-Si:H a suitable candidate for use as top cell in this configuration.

The integration of these CIGS and amorphous silicon cells in one monolithic stack faces several challenges. First of all, in conventional single junction amorphous silicon and micromorph solar cells illumination through the p-doped layer is favorable, as these cells are constraint by the drift length of the holes. In this novel device structure, the a-Si:H top cell is to be illuminated through the n-doped layer to align it with the configuration of the CIGS. Secondly, it is challenging to grow high-quality a-Si:H layers on the rough CIGS. The relatively sharp texture results in a-Si:H cell with a high shunt density. In addition, the amorphous silicon cell is current limiting. Increasing the light absorption of the top cell can significantly improve the performance of the tandem cell.

In this work, we demonstrate two approaches to tackle the above limitations to improve the performance of a-Si:H/CIGS tandem device. In the first approach, the CIGS cell is smoothened by mechanical polishing the ZnO interface. The smoother CIGS half fabricate facilitates the growth of a shunt-free a-Si:H top cell, increasing the V_{oc} and fill factor of the tandem cells. Very little related research to this methodology of interface smoothening can be found in literature. This concept has previously been demonstrated for micromorph solar cells where an intermediate i-ZnO layer [14] or nanocrystalline SiOx:H [14–16] has been polished. An extensive study of polishing ZnO built the framework for this research [17]. Mechanically polishing of layers on top of CIGS solar cells is unprecedented. Such smoothening approach induces additional challenges in terms of optimization, due to relative weak semiconductor-metal bonding.

The second approach is based on texturing of the ZnO:Al front electrode to enhance the generated photocurrent in the top sub-cell by forward scattering. Texturing of TCOs is a well-known strategy for light management in photovoltaic devices [18,19]. In this work, a wet-etching procedure is used for creating a textured front TCO surface. When a TCO is subject to an acid, the acid starts to react with the material, along its surface. Due to the columnar growth of TCOs, the acid will also penetrate partially along the grain boundaries and voids and etch the bulk of the material. Due to etching along the increased surface area at the grain boundaries, a inhomogeneous lateral etching speed is realized and a textured surface is realized. Likewise, when the acid penetrates and etches inside the voids, these develop into relatively larger craters. Wet-etching a TCO using this procedure, creates random textures that induce light scattering and improve light incoupling. By varying the type of TCO, deposition parameters, and etchants, one can alter the type of textures.

2. Methodology

2.1. Fabricating bottom sub-cell

The half fabricate comprises the glass substrate, molybdenum back contact, CIGS absorber layer, CdS buffer layer and the intrinsic ZnO (glass/Mo/CIGS/CdS/i-ZnO). A 1 mm thick sodalime glass substrate was cleaned in five steps. Firstly, it was scrubbed clean using isopropanol on tissue, followed by immersion in 4 consecutive baths of 10 min; first an ultrasonic bath of acetone; secondly an ultrasonic bath of isopropanol, followed by two baths of HNO_3 (a 99% HNO_3 bath at room temperature, and a 69% HNO_3 bath at 100 °C). After these steps the substrates are extensively rinsed with de-ionized water (DI water).

A 420 nm layer of molybdenum was sputtered on this substrate in two pressure steps. First, a more porous layer to adhere well to the substrate was deposited, followed by a more dense layer to form a well-conducting back contact. A 1 µm CIGS was deposited using three-stage-co-evaporation. During the CIGS deposition, the sodium diffuses into the CIGS layer through natural diffusion from the substrate. The first stage was processed at 400 °C, stage II and III at 550 °C. No post-

deposition treatments were performed. The 70 nm CdS was deposited by 6-min chemical bath deposition at 65 °C, using the precursors thiourea and $CdSO_4$, and NH_3 as a complexing agent.

A 500 nm thick i-ZnO layer was deposited using room temperature RF sputtering. The substrates were mounted on a moving carrier that passes by a rectangular sputtering target at 7 cm/min such that during a single pass about 50 nm of i-ZnO is deposited. For a 500 nm thick i-ZnO, 10 consecutive passes of the carrier were carried out.

2.2. Polishing

The half fabricate (glass/Mo/CIGS/CdS/i-ZnO) with (natural) rough surface morphology was cut in samples with a size of 2.5 × 2.5 cm. The samples were mechanically polished using non-dry polishing fluid and a 200 mm diameter chempolishing pad. The rotational speed both the mounting head and the table was set to 150 RPM, rotating in opposite directions. The applied downward forces were set to 10 N or 20 N, resulting in 16 kPa and 32 kPa pressure, respectively. Using these two pressures, polishing times were varied. After polishing, the slurry was removed from the surface by scrubbing with acetone and DI-water. These smoothened half fabricates have been characterized with an atomic force microscope and inspected with cross sectional scanning electron microscopy (SEM).

2.3. Fabrication of the top sub-cell

The top subcells were fabricated in a PE-CVD cluster tool having dedicated chambers for layers with different types of doping. Firstly, a 30 nm of phosphorus doped hydrogenated nanocrystalline SiOx:H (p-nc-SiO_x:H) was deposited. This was followed by two nanocrystalline SiOx: H, layers of 7 nm and 14 nm in thickness with different doping concentrations. The first p-nc-SiO_x:H layer (with a narrower bandgap) serves as part of the tunnel recombination junction. The following layer was a wider bandgap p-layer to serve as hole-collector in the top sub-cell. After deposition of the amorphous silicon, another 30 nm n-type nanocrystalline n-nc-SiO_x:H was deposited, and the cell is completed by RF sputtering an ZnO:Al 250 nm front electrode. As a final step, a 300 nm Ag front grid was evaporated on the devices. The short circuit current of these devices was determined with by EQE, and V_{oc} and FF with a triple A rated JV tester, calibrated with calibration diodes from the Fraunhofer ISE institute.

2.4. Texturing of the front electrode

In this work, the ZnO:Al front electrode has been wet-etched to create a front texturing. Regarding the experimental design, it is crucial that there is a full area coverage of ZnO:Al, as the 250 nm of ZnO:Al (after etching) serves as a protective layer, preventing any water and acid ingression to the cells underneath. The deposition pressures have been varied between 1.5 µbar, 2.5 µbar, and 3.5 µbar and deposition temperatures between 100 °C, 125 °C, and 150 °C. Higher temperatures are unsuitable in this architecture, considering that ZnO:Al is the final layer to be processed in these devices and higher temperatures would induce undesired diffusion of cadmium. In all cases etching was done in a 0.5% HCl bath for 45 s. After etching, the sample was rinsed for at least 3 min in DI water. The initially deposited thicknesses of ZnO:Al were optimized as such that a 250 nm layer of textured ZnO:Al remained after etching. As the etching rate was dependent on the deposition parameters, the initial thicknesses of the ZnO:Al was varied.

3. Results

3.1. Polishing

The deposition of the 500 nm i-ZnO layer was performed in 10 consecutive passes of the carrier by the sputtering target. This
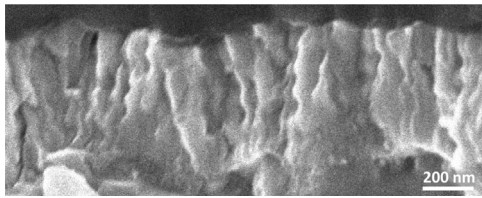
Fig. 1. Detail of a SEM cross-section of an i-ZnO layer, showing some wiggle-like structure due to the deposition conditions.

procedure has an effect on the growth of the crystal structure as shown in Fig. 1 below. The crystal structure is still showing continuous columnar growth as is expected for state-of-the art ZnO layer. However, an interesting artifact is observed induced by the movement of the carrier relative to the sputtering target. Fig. 1 shows that a wiggle structure is created.

During the mechanical polishing procedure, it is important to secure that the i-ZnO layer is not fully removed. A fully removed i-ZnO would risk a partly or full removal of the underlying CdS layer as well. A damaged CdS layer would deteriorate the cell performance. Thus, the removal rate is an essential variable. The removal rate (RR) was estimated using the modified Preston equation (Eq. (1)), compiled by Luo et al. [20]:

$$RR = K(P - P_{th})v + R_c. \tag{1}$$

In this equation the removal rate is expressed in terms of pressure (P), linear velocity (v) and the following constants; the Preston constant (K), a pressure constant (P_{th}), and a removal constant (R_c). Gupta et al. [17] determined empirically that for polishing i-ZnO these constants should be to be $K = 2.69 \cdot 10^{-4} \, Pa^{-1}$, $P_{th} = 1.235 \cdot 10^4 \, Pa$ and $R_c = 9 \, Å/min$, respectively. Using these values the initial removal rate was been estimated to be $RR = 209 \, nm/min$.

After polishing, the thickness was determined using SEM. The removal rates have been verified using 500 nm thick i-ZnO layer on Asahi-VU substrates. In Fig. 2 the cross-sectional SEM images of the unpolished and polished ZnO are displayed. In addition, an isometric overview of the polished sample is shown in Fig. 2(c). The dashed line in Fig. 2(b) indicates the very smooth interface and surface morphology of the polished interface. Some pinholes are observed in the isometric SEM image. These pinholes are assumed to reflect the pre-existing voids in the i-ZnO layer. The removal rate was determined to be $204 \pm 30.3 \, nm/min$, and thus consistent with removal rates reported in literature [17].

The mechanical polishing process was repeated on a CIGS bottom cells (glass/Mo/CIGS/CdS/i-ZnO). The surface morphology of these (un)polished interfaces were characterized using an atomic force microscope and the obtained RMS roughness is tabulated in Fig. 3 below. The decaying trends are correlated to the applied pressure and polishing time. Polishing for 60 s with 20 N downward force resulted in an
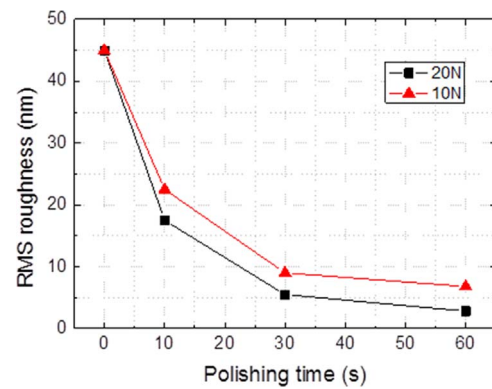

Fig. 3. Decaying trend in RMS roughness with increasing polishing times, using various pressures. Despite the differences in substrate material and initial RMS roughness, the minimum RMS roughness found is 6.6 nm and 2.8 nm for 10 and 20 N force respectively.

impressive low RMS roughness of 2.80 nm. From experience, longer polishing times than 60 s are inadvisable to be used. Longer polishing times induced some unwelcome edge effects such as peeling off of the CIGS layer.

Fig. 4 shows cross-sectional SEM images of hybrid tandem devices that have been fabricated. In Fig. 4(a) a reference tandem cell with a thick i-ZnO layer is displayed. Many lines appearing can be observed in the a-Si:H absorber layer of the top cell. These lines represent cracks in the amorphous silicon. In Fig. 4(b), the i-ZnO is polished, and a very smooth and flat interface is created. Hardly any inhomogeneity is observed in the post-deposited amorphous silicon layer.

Looking at the external parameters (Table 1 and Fig. 5a) one can see that especially the V_{oc} strongly increased after polishing. We think that this enhancement is partially induced by the thinner ZnO layer, and partially due to the better growth conditions for the amorphous silicon. As the V_{oc} of the polished device is very close the summation of the V_{oc} of the single junctions (800–850 mV and 610–630 mV for a-Si:H and CIGS, respectively) and no significant impact is observed in the fill factor, we conclude that the electrical performance is not significantly affected and we successfully polished an intermediate interface in these devices.

Regarding the spectral response of these solar cells (Fig. 5b), it is observed that polishing the interface significantly increases the interference. This significantly influences the spectral response of the bottom cell. However, as this layer is not current-limiting, this does not reflect in the device performance.

3.2. Textured ZnO:Al

The front electrode ZnO:Al was fabricated in the cluster-tool, with a stationary substrate holder. Hence, after the incubation phase of this columnar growth of this layer, a homogenous growth is expected. Fig. 6
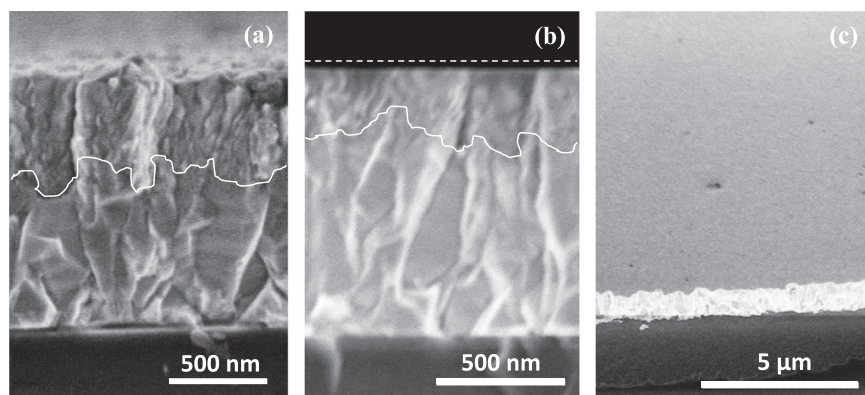

Fig. 2. (a) A cross sectional SEM image of the unpolished i-ZnO. (b) A cross sectional SEM image of the polished i-ZnO. The white dashed line indicates the polished interface. In Fig. 2(a) and (b) the white continuous line indicates the interface between the Asahi-VU and the ZnO. (c) An isometric SEM image of the polished ZnO. The dark spots indicate pinholes in the i-ZnO.
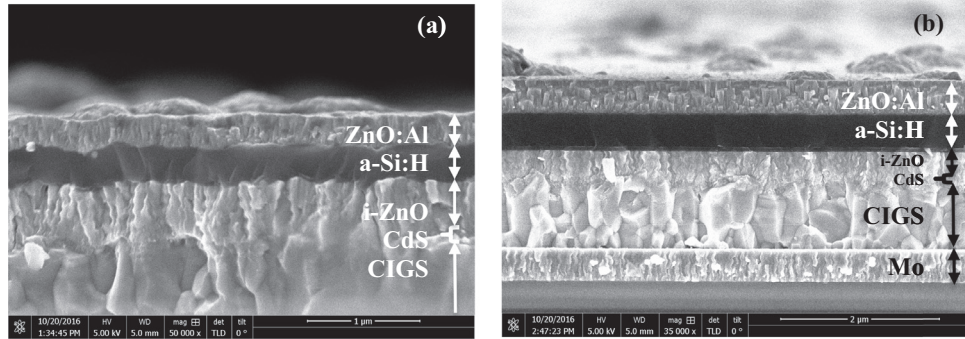
Fig. 4. (a) Cross-section of a tandem cell with a thick intermediate ZnO layer. (b) Cross-sectional SEM image of a complete hybrid tandem device with a polished intermediate i-ZnO layer.

Table 1
External parameters unpolished and polished tandem devices.

Tandem device	V_{oc} (mV)	FF (%)	J_{sc} (mA/cm^2)	η (%)
Unpolished	1.33	58.4	9.7	7.50
Polished	1.44	59.5	10.3	8.16

shows a scatter plot of the measured RMS roughness versus the measured correlation length of the various surface textures of the several varied parameters. In this figure, the contours indicate the aspect ratio of the surface texture, which is defined as the ratio between the RMS roughness and the correlation length. The higher the aspect ratio, the larger the forward scattering in the visible spectral range can be expected.

Upon reducing the deposition pressure (star – triangle – square) an increasing spread of values for the correlation length is observed. We explain this relation by the fact that a highly energetic precursor can induce defects and vacancies sub-surface in the bulk of the growing layer. At higher deposition pressures, the precursor atoms and ions experience more collisions with the argon atoms on their path towards the surface. Consequently, the atoms arrive at the surface with less energy, leading to layers with a higher density.

During the wet-etching process, denser films result in a more homogeneous lateral etching, due to dominance of etching along the surface rather than along the grain boundaries. As the films deposited at lower deposition pressures contain more voids, which the acid can penetrate along the grain boundaries, leading to more bulk etching and as a consequence larger features and correlation lengths.

In addition, Fig. 6 reveals the dependence on the substrate temperature during the ZnO:Al deposition. It shows that the higher the
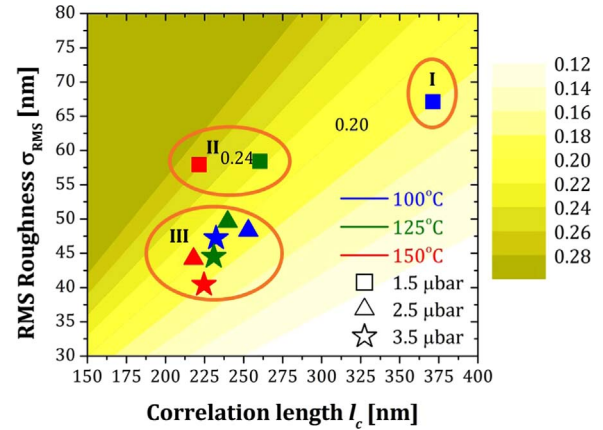

Fig. 6. RMS roughness and correlation length of different AZO combinations. The contour plot shows aspect ratio values. The orange circles show 3 different regimes for different deposition parameters.

substrate temperature, the less the correlation length is affected by etching. We believe that deposition at higher substrate temperatures leads to higher mobility of the precursor species at the surface of the film leading to denser films. Denser films means that the role of bulk etching versus surface etching is reduced and consequently its effect on the correlation length.

As a result of these different effects the different processing conditions lead to three different regimes of surface morphology. One regime with high RMS roughness & large correlation length (I), one regime with high RMS roughness and smaller correlation lengths (II) leading to the highest aspect ratio. The last regime corresponds to most of the dense films that are clustered in Fig. 6 in the parameter space with
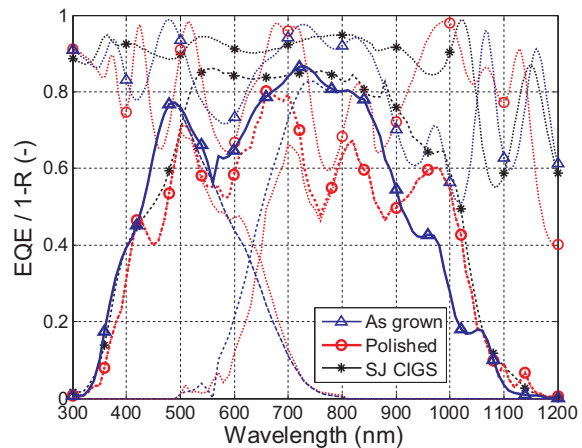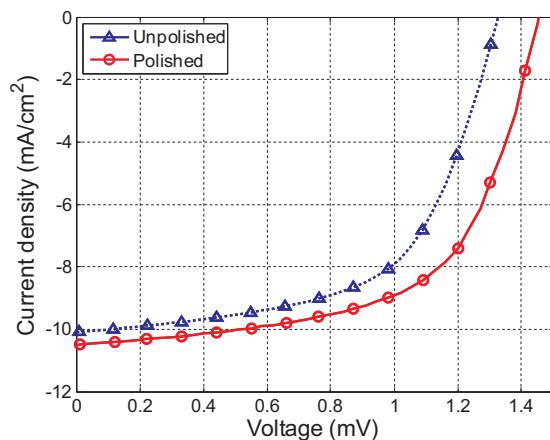

Fig. 5. (a) JV curves of an unpolished tandem cell with a thick intermediate ZnO layer (blue) and a polished solar cell (red) deposited in the same batch (b) EQE and 1-reflection measurements of a reference single junction CIGS cell (black), a reference tandem architecture (blue) and a polished device (red).
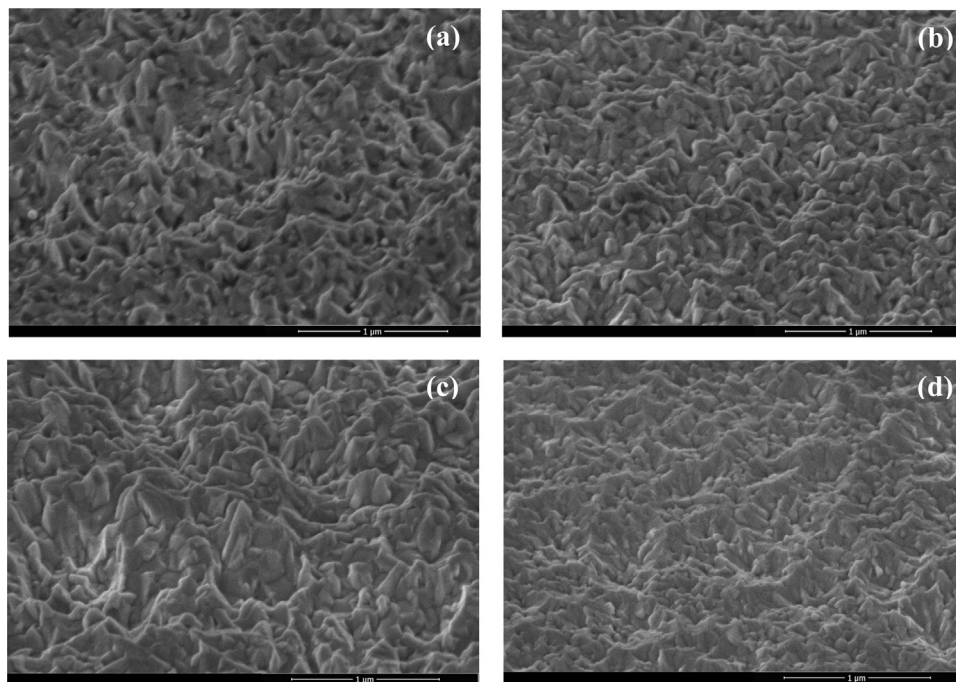
Fig. 7. SEM images of the 4 outer boundaries of the textured layers. (a) 100 °C and 1.5 µbar (b) 100 °C and 3.5 µbar (c) 150 °C and 1.5 µbar (d) 150 °C and 3.5 µbar.

small correlation lengths and limited RMS roughness (regime III).

These propositions are supported by Fig. 7. The SEM images show four surfaces of wet-etched ZnO:Al, where the ZnO:Al was deposited at various substrate temperatures and pressures. The surface morphology in Fig. 7(a) corresponds to ZnO:Al deposited at both the lowest temperature and pressure (regime I). The dark spots observed in the ZnO:Al (a) are an indication of the voidy nature of this film. Images 7(b) and 7(c) visually show comparable surface morphology, with significant less dark spots. The SEM image depicted in Fig. 7(d), supports that combining a high temperature with high deposition pressure (regime II) leads to a more compact film and more surficial etching. This is revealed by the textures in this image being significantly more alike oriented when compared to the 7(a)-(c).

The best light trapping is expected for textured ZnO:Al with the combination of highest RMS roughness and a correlation length close to the thickness of the absorber layer of the top cell (250–300 nm), favoring the ZnO:Al deposited at a pressure of 1.5 µbar at 150 °C. Fig. 8(a) shows that all textures significantly improve the J_{sc} of the devices. Additionally, one see that there is some spread in the V_{oc} between the

different textures. However, this is considered to be due to processing conditions, supported by the fact that also the 'as grown' reference device also has a fairly limited electrical performance.

For describing the light management qualities of these different textures it is more valuable to focus on overall device reflection (which can reduced by better light incoupling) and reduced coherence (indicating better light scattering). Fig. 8(b) shows how three of the textures (from the different regimes) affect the solar cell reflectance. Data of several textures is also summarized in Table 2 below. This shows that it can be concluded that all textures will significantly improve light incoupling (4 – 5% absolute reduction in averaged solar cell reflectance) as well as decrease the coherence of the light. Furthermore, the texture fabricated from the AZO deposited at 1.5 µbar at 150 °C (from regime II) outperforms the other textures both in terms of having the lowest average reflection as well as the smallest standard deviation of the reflected light, indicating that this texture functions best to reduce the coherence of the light.

Fig. 9 shows the EQE and 1-R (where R is reflectance) of tandem a-Si:H/CIGS tandem cells. One tandem cell has the optimized textured
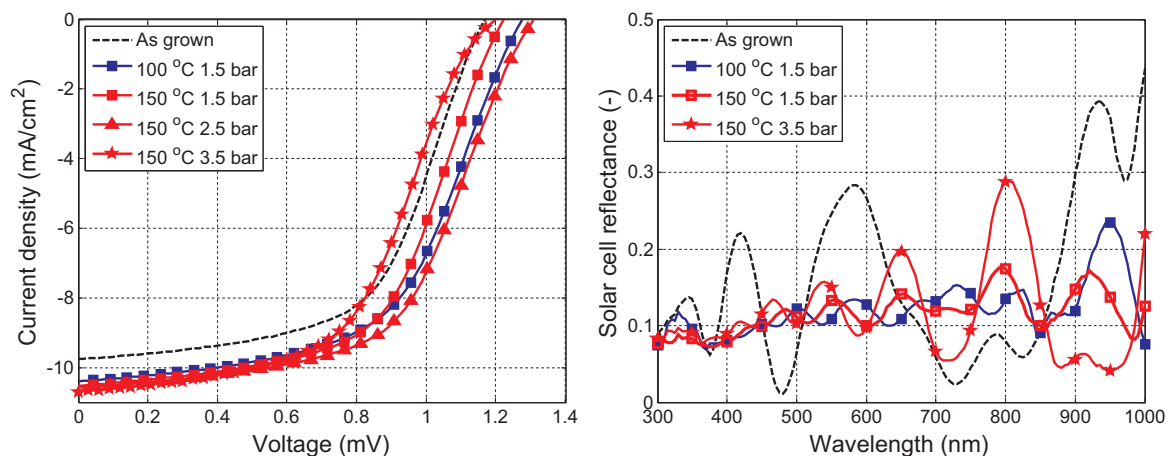

Fig. 8. (a) JV curves of tandem structures with AZO front electrodes with different textures, and an as grown reference (black dashed line) (b) Measured solar cell reflectance of the as grown reference and devices with surface morphologies from 3 different regimes.

Table 2

Averaged solar cell reflection and standard deviation for the as grown reference and textures from various regimes.

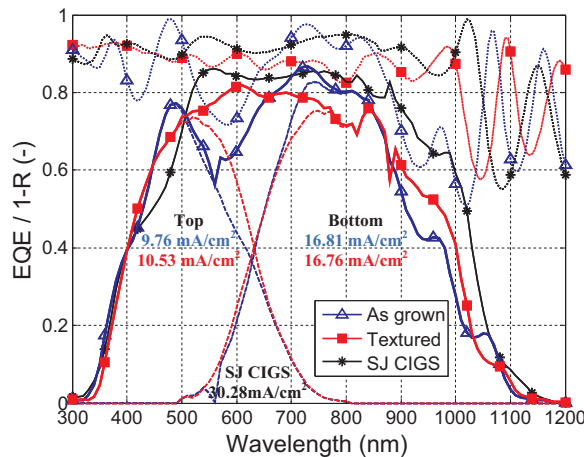| Deposition condition (textured AZO)	Device reflection (%) (averaged 0.3–1 μm)	Standard deviation
As grown	16.11	10.75
100 °C – 1.5 μbar	12.24	3.46
150 °C – 1.5 μbar	11.59	2.61
150 °C – 2.5 μbar	12.68	3.90
150 °C – 3.5 μbar	11.78	6.04

Fig. 9. EQE and 1-R of the hybrid tandem device with a textured front electrode (red), where the front electrode had been deposited with a deposition pressure of 1.5 μbar with a substrate temperature of 150 °C, compared with a reference device (black).

ZnO:Al (deposited at 150 °C at 1.5 μbar, indicated in red) and the reference cell has a front ZnO:Al without being exposed to an etching procedure (blue). Additionally, the parameters of a 1 μm single junction CIGS is displayed for comparison (black). Looking at the 1-R it becomes apparent that the coherence of the reflected light is significantly reduced when the front TCO is textured. This has the most effect in two spectral ranges. The first range (950–1050 nm), is around the band edge of CIGS. Please note, this is where the most optical losses appear in ultrathin CIGS layers. However, as currently the top sub-cell is current-limiting, this enhancement has no direct effect on the device performance. The other range (500–650 nm) significantly enhances the top cell performance, eliminating the destructive interference dip observed in the as grown tandem device. In these devices, the textured front TCO increased the current of the top sub-cell with 7.9% relatively to the reference. We expect to further improve current matching by further optimizing the top cell architecture.

4. Conclusions and discussion

We successfully integrated a mechanically polishing step for an intermediate i-ZnO layer in hybrid a-Si:H/CIGS tandem solar cells without damaging the electrical performance. Using this technique, working hybrid tandem devices have been presented. The RMS roughness of these polished i-ZnO layers have been reduced from 44 nm to 2.8 nm. The SEM images show that flattening the bottom half fabricate (glass/Mo/CIGS/CdS/i-ZnO) significantly improves the quality of the a-Si:H cell as no more cracks in the a-Si:H absorber layer are observed. More than 100 mV increase in V_{oc} has been measured compared to the unpolished tandem structure. We attribute this increase to both reducing the thickness of the i-ZnO and improved growth conditions for the top sub-cell. Furthermore, these extremely flat interfaces accommodate the research for implementation of an intermediate Bragg reflector to enhance the photogenerated current in the top sub-cell.

In addition, a texturing procedure of the front electrode of the a-Si:H/CIGS tandem solar cell has been developed. We demonstrated that we can manipulate the surface morphology of these textures by adjusting the parameters in the TCO deposition. These textures can successfully reduce the device reflectance, and an optical optimum has been found in 11.59 ± 2.61% reflection over a wavelength range of 300–1000 nm. As texturing our devices did not deteriorate the electrical and optical performance of our devices, we conclude that the front electrode can serve as a barrier against the acid treatment and water rinsing, protecting the cells underneath.

The demonstrated procedures are not solely applicable in architectures considering these type of the absorber layers, but with slight alterations many different types of multi-junction solar cells can benefit from these techniques. Therefore, this work can be considered as a fundamental study that can contribute to work towards high quality monolithic two-terminal hybrid tandem solar cells.

References

[1] M. Green, K. Emery, Y. Hishikawa, W. Warta, Solar cell efficiency tables (version 34), Prog. Photo.: Res. Appl. 17 (2009) 320–326.

[2] H. Sai, T. Matsui, T. Koida, K. Matsubara, M. Kondo, S. Sugiyama, H. Katyama, Y. Takeuchi, I. Yoshida, Triple-junction thin-film silicon solar cell fabricated on periodically textured substrate with a stabilized efficiency of 13.6%, Appl. Phys. Lett. 106 (2015) 213902.

[3] F.T. Si, O. Isabella, H. Tan, M. Zeman, Quadruple-Junction thin-film silicon solar cells using four different absorber, Mater., Sol. R. R. L. 1 (2017) 1700036.

[4] B. Liu, L. Bai, T. Li, W. Changchun, B. Li, Q. Huang, D. Zhang, G. Wang, Y. Zhao, X. Zhang, High efficiency and high open-circuit voltage quadruple-junction silicon thin film solar cells for future electronic applications, Energy Environ. Sci. 10 (2017) 1134.

[5] A. Hadipour, B. De Boer, P.W.M. Blom, Organic tandem and multi-junction solar cells, Adv. Funct. Mater. 18 (2008) 169–181.

[6] C.-C. Chen, W.-H. Chang, K. Yoshimura, K. Ohya, J. You, J. Gao, Z. Hong, Y. Yang, An efficient triple-junction polymer solar cell having a power conversion efficiency exceeding 11%, Adv. Mater. 26 (2014) 5670–5677.

[7] J.P. Mailoa, C.D. Bailie, E.C. Johlin, E.T. Hoke, A.J. Akey, W.H. Nguyen, M.D. McGehee, T. Buonassisi, A 2-terminal perovskite/silicon multijunction solar cell enabled by a silicon tunnel junction, Appl. Phys. Lett. 106 (2015) 121105.

[8] S. Essig, M.A. Steiner, C. Allebe, J.F. Geisz, B. Paviet-Salomon, S. Ward, A. Descoeudres, V. La Salvia, L. Barraud, N. Badel, A. Faes, J. Levrat, M. Despeisse, C. Ballif, P. Stradins, D.L. Young, Realization of GaInP/Si dual-junction solar cells With 29.8% 1-Sun efficiency, IEEE J. Photovolt. 6 (2014) 4.

[9] S.Y. Chae, S.J. Park, O.-S. Joo, U.Y. Jun, B.K. Min, Y.J. Hwang, Highly stable tandem solar cell monolithically integrating dye-sensitized and CIGS solar cells, nature, Sci. Rep. 6 (2016) 30868.

[10] L. Kranz, A. Abate, T. Feurer, F. Fu, E. Avancini, J. Löckinger, P. Reinhard, S.M. Zakeeruddin, M. Grätzel, S. Buecheler, A.N. Tiwari, "High-Efficiency Polycrystalline Thin Film Tandem Solar Cells, J. Phys. Chem. Lett. 6 (2015) 2676–2681.

[11] Karlsruhe Institute of Technology, Record for perovskite/CIGS tandem solar module, SD, 27 September 2016.

[12] B. Vermang, V. Fjällström, J. Petterson, P. Salomé, M. Edoff, Development of rear surface passivated Cu(In,Ga)Se2 thin film solar cells with nano-sized local rear point contacts, Sol. Energy Mater. Sol. Cells 117 (2013) 505–511.

[13] a. Duchalet, E. Letty, S. Jaime-Ferrer, P.-P. Grand, F. Mollica, N. Naghavi, The impact of reducing the thickness of electrodeposited stacked Cu/In/Ga layers on the performance of CIGS solar cells, Sol. Energy Mater. Sol. Cells 162 (2017) 114–119.

[14] P. Babál, Doped nanocrystalline silicon oxide for the use as (intermediate) reflecting layers in thin-film silicon solar cells, Ph.D. Thesis Delft University of Technology, 2014.

[15] M. Boccard, Novel Micromorph Solar Cell Structures for Efficient Light Trapping and High-Quality Absorber Layers, PhD thesis, EPFL (2012).

[16] P. Cuony, Optical Layers for Thin-film Silicon Solar Cells, PhD thesis, EPFL, 2011.

[17] S. Gupta, P. Kumar, A.A. Chakkaravathi, D. Craciun, R.K. Singh, Investigation of chemicalmechanical polishing of zinc oxide thin films, Appl. Surf. Sci. 257 (2011) 5837–5843.

[18] O. Kluth, B. Rech, L. Houben, S. Wieder, G. Schöpe, C. Beneking, H. Wagner, A. Löffl, H.W. Schock, Texture etched ZnO:Al coated glass substrates for silicon based thin film solar cells, Thin Solid Films 351 (1999) 247–253.

[19] J. Krc, M. Zeman, O. Kluth, E. Smole, M. Topic, Effect of surface roughness of ZnO:Al films on light scattering in hydrogenated amorphous silicon solar cells", Thin Solid Films 426 (2003) 296–304.

[20] Q. Luo, S. Ramarajan, S.V. Babu, Modification of the Preston equation for the chemical mechanical polishing of copper, Thin Solid films 335 (1998) 160–167.